PHYSICAL REVIEW B VOLUME 51, NUMBER 6 1 FEBRUARY 1995-II

Theory of electron backscattering from crystals

S. L. Dudarev
Department of Materials, University of Oxford, Parks Road, Oxford OX1 3PH, United Kingdom

P. Rez
Department of Physics and Center for Solid State Science, Arizona State University, Tempe, Arizona 85287-1704

M. J. Whelan
Department of Materials, University of Oxford, Parks Road, Oxford OX1 3PH, United Kingdom
(Received 7 September 1994; revised manuscript received 24 October 1994)

The contrast in electron channeling patterns is quantitatively treated using a theory in which electrons in Bloch states excited by the incident electron are scattered through large angles by the fluctuation part of the potential (thermal diffuse scattering). The subsequent multiple elastic and inelastic scattering is described by an inhomogeneous transport equation. Formally this is shown to be identical to the solution of the kinetic equation for the one-particle spectral density matrix. Employing the supermatrix algorithm proposed by Fathers and Rez, we develop a computational technique which makes it possible to perform full-scale multiple scattering simulations of electron backscattering from crystals and to provide a consistent quantitative explanation of a number of experimental observations, including the dependence of the contrast on the detector position and on the energy of the backscattered electrons, the origin of which has not previously been fully accounted for. Our computational results show a substantial increase in the channeling contrast and in the signal-to-noise ratio for the conditions of oblique incidence and low takeoff angle of backscattering, which agrees with recent experimental studies. We show that under the conditions of multiple scattering there exists a perturbation expansion which considerably simplifies the problem of evaluation of the contrast and which can be employed for interpretation of channeling images of defects.

I. INTRODUCTION

Recent experimental observations[1,2] have demonstrated the possibility of direct imaging of defects in the bulk crystal using the so-called channeling mode in a conventional scanning electron microscope (SEM). The idea that images of this type could be obtained in practice was discussed by Booker *et al.*[3] soon after the experimental discovery of electron channeling patterns by Coates.[4] Channeling patterns arise in SEM's as a result of variation of the coefficient of backscattering of electrons with change in the orientation of the incident beam with respect to the atomic planes of the crystal. A dislocation becomes visible due to local bending of the atomic planes, which results in a variation of the coefficient of backscattering when the beam of incident electrons scans over the region corresponding to the distortion of the lattice.[5,6]

A formulation by Hirsch and Humphreys[7] and by Vicario *et al.*[8] of the first theoretical models capable of providing a description to the contrast effects associated with electron channeling showed that in order to obtain quantitative results, it is essential to take into account multiple inelastic scattering of electrons. Reimer, Badde, and Seidel,[9] and Clark and Howie[10] developed theoretical methods which made possible to evaluate the *variation* of the backscattering coefficient with changing the direction of incidence, and in the last case the authors extended the theory to consideration of imperfect crystals. Spencer, Humphreys, and Hirsch[11] emphasized the importance of a consistent treatment of the effects of multiple scattering of electrons in the crystal bulk, and proposed the so-called forward-backward approximation in which all the inelastically scattered electrons were separated into two groups moving in opposite directions normal to the surface. In the treatments quoted above the effect of energy losses has been taken into account in a semiempirical way by introducing some adjustable parameters. Sandström, Spencer, and Humphreys[12] generalized the approach developed in Ref. 11 in order to be able to calculate energy spectra of electrons backscattered from crystals. Discussing the limitations of the approach developed in Refs. 11, 12, Howie[13] noted that the forward-backward approximation, although being relatively simple and convenient for carrying out many-beam dynamical diffraction calculations (see, e.g., recent results by Marthinsen and Høier[14]), ignores scattering through intermediate angles $\vartheta \sim \pi/2$ and therefore it may not be fully applicable to the interpretation of experimental observations performed using the geometry of oblique incidence of electrons on the surface,[15,16,1,2] for which the angular distribution of backscattered electrons and their energy spectrum depend strongly on the polar and the azimuthal angles of incidence.[17–20]

More recently, two alternative treatments have been proposed of the problem of multiple scattering of electrons by single crystals. One of them (see Ref. 16 and

21–23) is based on Monte Carlo simulations of electron backscattering. The other employs the transport equation.[24] Each of these approaches involves further simplifications; in particular the Monte Carlo formulation developed by Morin and co-workers[22,23] is based on the two-beam approximation of dynamical diffraction theory, while the treatment proposed by Spencer and Humphreys[24] employs the assumption that the effect of energy loss is equivalent to the condition that the crystal thickness is finite. In the present paper we formulate a method which is not restricted by these approximations, and which makes it possible to compute both the angular and energy distributions of backscattered electrons for any direction of incidence using many-beam dynamical diffraction theory.

The method which is described in the present paper is based on the kinetic equation for the one-particle density matrix. The idea that the density matrix formalism can be applied to the analysis of multiple inelastic scattering of charged particles by crystals has been proposed by Kagan and Kononets[25] and by Rez.[26] Recently it has been shown[27–29] that the kinetic equation for the spectral density matrix can be used for quantitative evaluation of the contribution of inelastically scattered electrons to the diffraction pattern observed in the transmission geometry of scattering. Dudarev, Vvedensky, and Whelan[30] have demonstrated how the density matrix approach can be applied to the treatment of dynamical electron diffraction from partially disordered growing surfaces. Below we use the density matrix formalism in order to describe high-energy electron backscattering from a bulk crystal. We show how under certain conditions the kinetic equation for the density matrix can be transformed and reduced to an inhomogeneous transport equation similar to that formulated by Spencer and Humphreys.[24] Within the framework of this model, elastic dynamical diffraction of the incident electrons is described using a Bloch wave formulation. Quasielastic phonon scattering results in attenuation of the intensity of Bloch waves and gives rise to a redistribution of intensity to larger angles of scattering. In what follows the electrons undergo multiple quasielastic (electron-phonon) and inelastic (electron-electron) scattering before emerging from the crystal. This process is best modeled using a transport equation. The dynamical diffraction and subsequent phonon scattering act as a source term. The large angle quasielastic scattering is represented by a Rutherford cross section; the inelastic scattering through small angles which includes plasmons, valence electrons, and inner shell excitations is described by an effective average cross section derived from the Bethe energy loss law. The processes included in our model and corresponding to various terms of the inhomogeneous transport equation (see below) are shown schematically in Fig. 1. Using a supermatrix algorithm proposed by Fathers and Rez,[31,32] we develop an efficient computational technique for solving this equation. The numerical results obtained demonstrate that the present approach provides a consistent explanation of a number of experimental observations, the interpretation of which has hitherto remained obscure in previous theoretical treatments. In what follows we use our approach in order to extend the perturbation treatment developed by Howie,[13] and prove that under conditions of multiple scattering there exists a simple approximate formula which can be employed for interpretation of electron channeling images of defects.

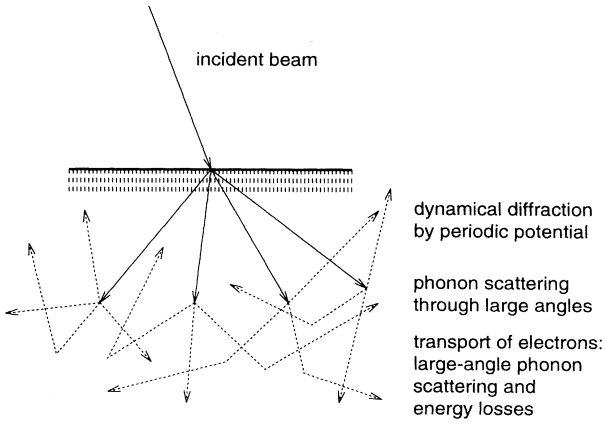

FIG. 1. Schematic diagram representing the basic stages of the process of backscattering of high-energy electrons from crystals.

II. TRANSPORT EQUATION

As was shown recently,[29] in order to evaluate the double differential cross section of inelastic scattering of high-energy electrons by a solid taking into account both the effects of dynamical diffraction and multiple inelastic interactions, one needs to find a solution of the kinetic equation for the so-called spectral one-particle density matrix $\rho(\mathbf{r},\mathbf{r}',E)$, the diagonal elements $\rho(\mathbf{r},\mathbf{r},E)$ of which give the probability distribution of finding an electron having the energy E at the point $\mathbf{r}$, while the off-diagonal elements are relevant to the distribution of scattered electrons over angle and energy. In principle

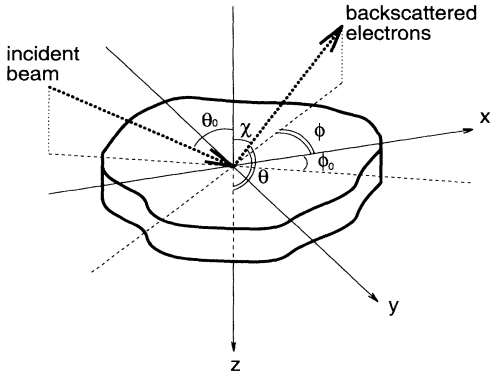

FIG. 2. Schematic diagram illustrating the geometry of scattering. The incident and backscattered beam directions are indicated with heavy dotted lines. The projections of these directions on the x,y plane are indicated by dashed lines.

the approach formulated in Ref. 29 makes it possible to calculate all the details of the cross section and, for example, to find the distribution of intensity in electron backscattering Kikuchi pattern.[33–35] However, in many cases information about the fine detail of the angular distribution of backscattered electrons is not required, and what is observed experimentally[1,2] is the intensity of backscattering averaged over a relatively large acceptance window of the detector, i.e., over a range of angles $(\Delta\theta, \Delta\phi)$ where both $\Delta\theta$ and $\Delta\phi$ are of the order of a few degrees (for the definition of the geometry of scattering see the diagram shown in Fig. 2). This considerably simplifies the treatment and makes it possible to neglect the influence of dynamical diffraction on the distribution of electrons *emerging* from the crystal (it does not simplify the treatment of diffraction of the *incident* electrons). The incident electrons are dynamically diffracted by the static crystal potential and inelastically scattered through small angles. This group of electrons is best represented by the appropriate Bloch functions whose flux is depleted by scattering to large angles by the fluctuation part of the crystal potential (thermal diffuse or large angle phonon scattering). The subsequent multiple elastic and inelastic scattering of these electrons can be treated using a transport equation in the same way as for electrons incident on a semi-infinite amorphous medium. Mathematically the process can be represented by an inhomogeneous transport equation, where the phonon-scattered electrons from the Bloch wave states act as a source term, viz.,

$$v\mathbf{n}\frac{\partial}{\partial \mathbf{r}}F(\mathbf{n},E,\mathbf{r}) = n_V \int do_{\mathbf{n}'} \int d\varepsilon \frac{d^2\sigma}{do_{\mathbf{n}'}d\varepsilon}\left(\mathbf{n},E\middle|\mathbf{n}',E+\varepsilon\right)v'F(\mathbf{n}',E+\varepsilon,\mathbf{r})$$
$$-n_V \int do_{\mathbf{n}'} \int d\varepsilon \frac{d^2\sigma}{do_{\mathbf{n}'}d\varepsilon}\left(\mathbf{n}',E-\varepsilon\middle|\mathbf{n},E\right)vF(\mathbf{n},E,\mathbf{r}) + Q(\mathbf{n},E,\mathbf{r}). \tag{1}$$

In this equation $F(\mathbf{n},E,\mathbf{r})$ denotes the distribution function which is proportional to the probability of finding an electron at the point $\mathbf{r}$ moving along the direction

$$\mathbf{n} = (\sin\theta\cos\phi, \sin\theta\sin\phi, \cos\theta),$$

n_V is the number of atoms per unit volume, and $v = \sqrt{2E/m}$ is the velocity of the electron. The quantity $d^2\sigma\left(\mathbf{n},E\middle|\mathbf{n}',E+\varepsilon\right)/do_{\mathbf{n}'}d\varepsilon$ is the double differential cross section of scattering of an electron from the state characterized by the direction of motion $\mathbf{n}'$ and the energy $E+\varepsilon$ to the state $(\mathbf{n},E)$ by the *fluctuation part* of the potential of a single atom which is associated with thermal vibrations and excitations of the electronic subsystem of the crystal. The source function $Q(\mathbf{n},E,\mathbf{r})$ on the right-hand side of Eq. (1) describes electrons which have undergone inelastic scattering through relatively large angles (i.e., the angles exceeding the Bragg angle). Application of an inhomogeneous transport equation to the problem of electron backscattering by crystals was considered by Spencer and Humphreys.[24] Recently, Werner, Tilinin, and Hayek[36] have shown how an inhomogeneous transport equation can be applied to the description of electron backscattering from amorphous solids.

Equation (1) can be formally derived from the quantum kinetic equation under the assumption that the scattering from the small-angle Bloch wave group of electrons into the group of electrons scattered through large angles is a first-order process. As follows from the derivation given in Appendix A, there exists an explicit expression for the source function $Q(\mathbf{n},E,\mathbf{r})$ entering Eq. (1), namely,

$$Q(\mathbf{n},E,\mathbf{r}) = v\left(\frac{m}{2\pi\hbar^2}\right)^2 \int\int_{|\mathbf{r}-\mathbf{x}|,|\mathbf{r}-\mathbf{x}'|\sim r_0} d^3x d^3x' \exp[i\mathbf{k}\cdot(\mathbf{x}'-\mathbf{x})] \int d\omega\, \bar{s}(\mathbf{x}',\mathbf{x},\omega)\rho_{\mathrm{SA}}(\mathbf{x},\mathbf{x}',E+\hbar\omega), \tag{2}$$

in which $\mathbf{k} = \mathbf{n}mv/\hbar$ is the wave vector, $\rho_{\mathrm{SA}}(\mathbf{x},\mathbf{x}',E+\hbar\omega)$ is the density matrix describing the electrons scattered through small angles (i.e., describing the first stage of the process shown in Fig. 2), $\bar{s}(\mathbf{x}',\mathbf{x},\omega)$ is the mixed dynamic form factor of localized inelastic interactions, and r_0 is a parameter defined in Appendix A. In accordance with the derivation given in Appendix A, integration over $\mathbf{x}$ and $\mathbf{x}'$ on the right-hand side of this expression should be carried out over the vicinity of the point $\mathbf{r}$.

Equations (1) and (2) form the basis of our treatment, and in what follows we intend to develop a method which is suitable for solving these equations. We start from the definition of the basic quantities entering (1) and (2). In the case of phonon scattering the dynamic form factor can be represented in the form[11,37]

$$\bar{s}(\mathbf{x},\mathbf{x}',\omega) = \delta(\omega)\sum_a \int\int \frac{d^3q d^3q'}{(2\pi)^6} U_a(\mathbf{q})U_a(-\mathbf{q}')\exp[i\mathbf{q}\cdot(\mathbf{x}-\mathbf{r}_a) - i\mathbf{q}'\cdot(\mathbf{x}'-\mathbf{r}_a)]$$
$$\times\{\exp[-M_a(\mathbf{q}-\mathbf{q}')] - \exp[-M_a(\mathbf{q}) - M_a(\mathbf{q}')]\}, \tag{3}$$

where $U_a(\mathbf{q})$ denotes the Fourier component of the potential of a single atom, $M_a(\mathbf{q}) = \langle(\mathbf{q}\cdot\mathbf{u}_a)^2\rangle/2$ is the Debye-Waller factor, and $\mathbf{u}_a$ is the thermal displacement of an atom a. Summation over a in (3) is carried out over all atoms of the crystal. If we disregard the effect of damping of coherence in the process of small-angle scattering by collective electronic excitations, then the density matrix $\rho_{sa}(\mathbf{x},\mathbf{x}',E)$ can be written in the form of a sum of propagating and diffracted waves with slowly varying amplitudes,

$$\rho_{\mathrm{SA}}(\mathbf{x},\mathbf{x}',E)=\delta(E-E_0)\sum_{h,l}\phi_h(\mathbf{x})\phi_l^*(\mathbf{x}')\exp[i(\mathbf{k}_0+\mathbf{G}_h)\cdot\mathbf{x}]\exp[-i(\mathbf{k}_0+\mathbf{G}_l)\cdot\mathbf{x}'], \tag{4}$$

where the summation is carried out over the reciprocal lattice vectors of the crystal $\mathbf{G}_h$ and $\mathbf{G}_l$, and $\mathbf{k}_0$ is the wave vector of the incident electrons. Each of the amplitudes $\phi_h(\mathbf{x})$ entering (4) satisfies the Schrödinger equation of the form[38] (the so-called Takagi equation)

$$i\frac{\hbar^2}{m}(\mathbf{k}_0+\mathbf{G}_h)\cdot\nabla_{\mathbf{x}}\phi_h(\mathbf{x})=\frac{\hbar^2}{2m}\left[(\mathbf{k}_0+\mathbf{G}_h)^2-\mathbf{k}_0^2\right]\phi_h(\mathbf{x})+\sum_t\left(U_{ht}-\frac{i}{2}\gamma_{ht}\right)\phi_t(\mathbf{x}), \tag{5}$$

which relates the functions $\phi_h(\mathbf{x})$ for various h. In Eq. (5) the quantities U_{ht} denote the Fourier components of the periodic potential of the crystal,

$$U_{ht}=U(\mathbf{G}_h-\mathbf{G}_t)=\frac{1}{\Omega}\sum_\alpha U_\alpha(\mathbf{G}_h-\mathbf{G}_t)\exp[-i(\mathbf{G}_h-\mathbf{G}_t)\cdot\mathbf{r}_\alpha]\exp[-M_a(\mathbf{G}_h-\mathbf{G}_t)], \tag{6}$$

where Ω denotes the volume of a unit cell, and matrix elements γ_{ht} represent non-Hermitian corrections to these quantities which result from inelastic interactions, namely,[39]

$$\begin{aligned}\gamma_{ht}=\frac{1}{\Omega}\sum_\alpha\int\frac{d^3q}{(2\pi)^2}\delta\left(E_0-\frac{\hbar^2\mathbf{q}^2}{2m}\right)U_\alpha(\mathbf{k}_0+\mathbf{G}_h-\mathbf{q})U_\alpha(\mathbf{q}-\mathbf{k}_0-\mathbf{G}_t)\exp[-i(\mathbf{G}_h-\mathbf{G}_t)\cdot\mathbf{r}_\alpha]\\ \times\{\exp[-M_\alpha(\mathbf{G}_h-\mathbf{G}_t)]-\exp[-M_\alpha(\mathbf{k}_0+\mathbf{G}_h-\mathbf{q})-M_\alpha(\mathbf{k}_0+\mathbf{G}_t-\mathbf{q})]\}.\end{aligned} \tag{7}$$

Substituting (4) and (3) into (2), we arrive at an explicit expression for the source function,

$$\begin{aligned}Q(\mathbf{n},E,\mathbf{r})=v\left(\frac{m}{2\pi\hbar^2}\right)^2\delta(E-E_0)\frac{1}{\Omega}\sum_\alpha\sum_{h,l}\phi_h(\mathbf{r})\phi_l^*(\mathbf{r})\\ \times U_\alpha(\mathbf{k}_0+\mathbf{G}_h-\mathbf{k})U_\alpha(\mathbf{k}-\mathbf{k}_0-\mathbf{G}_l)\exp[-i(\mathbf{G}_l-\mathbf{G}_h)\cdot\mathbf{r}_\alpha]\\ \times\{\exp[-M_\alpha(\mathbf{G}_l-\mathbf{G}_h)]-\exp[-M_\alpha(\mathbf{k}_0+\mathbf{G}_h-\mathbf{k})-M_\alpha(\mathbf{k}_0+\mathbf{G}_l-\mathbf{k})]\},\end{aligned} \tag{8}$$

in which $\mathbf{k}$ denotes the wave vector of the electron after inelastic scattering, $\mathbf{k}=k\mathbf{n}=\sqrt{2mE/\hbar^2}\,\mathbf{n}$.

It can be expected that the source function (8) satisfies the requirement of current conservation, i.e., that the total current generated by this source function must be the same as the current associated with the incident beam of electrons. Indeed, combining Eqs. (1), (7), and (8), and taking into account the condition that $dE=(\hbar^2/m)kdk$, we obtain

$$\begin{aligned}\nabla_{\mathbf{r}}\int do_{\mathbf{n}}\int dE\;\mathbf{v}F(\mathbf{n},E,\mathbf{r})&=\int dE\int do_{\mathbf{n}}Q(\mathbf{n},E,\mathbf{r})\\ &=\frac{1}{\hbar}\sum_{h,l}\gamma_{hl}\phi_l(\mathbf{r})\phi_h^*(\mathbf{r})=-\frac{\hbar}{m}\sum_h(\mathbf{k}_0+\mathbf{G}_h)\cdot\nabla_{\mathbf{r}}|\phi_h(\mathbf{r})|^2.\end{aligned} \tag{9}$$

Integrating (9) over the volume of the crystal, we arrive at equation

$$\int_V d^3r\int dE\int do_{\mathbf{n}}Q(\mathbf{n},E,\mathbf{r})=-\int_S d\mathbf{S}\left[\frac{\hbar}{m}\sum_h(\mathbf{k}_0+\mathbf{G}_h)|\phi_h(\mathbf{r})|^2\right], \tag{10}$$

which shows that the total flux generated by the source function $Q(\mathbf{n},E,\mathbf{r})$ in the transport equation (1) is equal to the decrease of the flux associated with electrons scattered through small angles. Integration over $\mathbf{S}$ is carried out over an arbitrary closed surface surrounding the crystal. It is important to emphasize that condition (10) is satisfied for any direction of incidence, and this fact will be used below in order to formulate a perturbation scheme for evaluation of the contrast of the channeling patterns.

III. NUMERICAL SOLUTION

In this section we describe briefly a numerical procedure which has been developed in order to solve Eq. (1) taking into account both quasielastic scattering and energy losses of the high-energy electrons. We assume that the crystal occupies the region $z>0$ and the boundary conditions are homogeneous in the plane $z=0$, i.e., $Q(\mathbf{n},E,\mathbf{r})=Q(\mathbf{n},E,z)$. As follows from the results obtained in the previous section, all the electrons are effectively generated inside the crystal by the source function (8), and so the distribution function $F(\mathbf{n},E,z)$ satisfies a homogeneous boundary condition at $z=0$ and $\mathbf{n}_z>0$,

$$F(\mathbf{n},E,z)\Big|_{z=0}=0\quad\text{for}\quad\mathbf{n}_z>0. \tag{11}$$

Introducing the flux density $N(\theta,\phi,E,z)$ instead of the distribution function $F(\mathbf{n},E,z)$ by the relation $N(\theta,\phi,E,z) = vF(\mathbf{n},E,z)$, we can rewrite Eq. (1) in the form

$$\cos\theta\frac{\partial}{\partial z}N(\cos\theta,\phi,E,z) = \int_{-\pi}^{\pi}d\phi'\int_{0}^{\pi}d\theta'\sin\theta' w_{\rm el}(\cos\psi',E)N(\cos\theta',\phi',E,z) + \frac{\partial}{\partial E}\left[\bar{\epsilon}(E)N(\cos\theta,\phi,E,z)\right] - w_{\rm el}^{(\rm tot)}(E)N(\cos\theta,\phi,E,z) + Q(\cos\theta,\phi,E,z), \tag{12}$$

where the angle ψ' between two directions of propagation $\mathbf{n}$ and $\mathbf{n}'$ is given by the formula

$$\cos\psi' = \sin\theta\sin\theta'\cos(\phi-\phi') + \cos\theta\cos\theta'$$

and where we have followed a standard procedure[40–42] and separated the double differential cross section of scattering $[d^2\sigma/do_{\mathbf{n}}d\varepsilon]$ into two parts, the first part describing quasielastic scattering and the second part representing the cross section of energy losses. It should be noted that this separation is not always possible. In particular, it is known that electron-electron scattering results both in energy losses *and* in a change in the direction of propagation.[43]

In our calculations we used the screened Rutherford formula for the probability of quasielastic scattering,

$$w_{\rm el}(\cos\psi,E) = n_V\left(\frac{Ze^2}{2E}\right)^2(1+\beta-\cos\psi)^{-2}, \tag{13}$$

where β was considered as an adjustable parameter. In the case of scattering by an amorphous medium the magnitude of this parameter was chosen to be $\beta = 1/2(ka_{\rm TF})^2$, where $a_{\rm TF} = 0.885a_B/Z^{1/3}$ is the Thomas-Fermi radius[44] and a_B is Bohr's radius. In the case of scattering by a crystalline material, where the cross section of quasielastic scattering depends on the absolute temperature,[45,46,24,47] the value of β was chosen in such a way as to obtain the best fit to the cross section of scattering by phonons. Integration of (13) over the entire solid angle gives the total probability of quasielastic scattering $w_{\rm el}^{(\rm tot)}(E) = n_V\sigma_{\rm el}^{(\rm tot)}(E) = 4\pi n_V(Ze^2/2E)^2[\beta(2+\beta)]^{-1}$. The average rate of energy losses, $\bar{\epsilon}(E)$, in Eq. (12) is assumed to follow the Bethe law[48] $\bar{\epsilon}(E) = (2\pi n_V Ze^4/E)\ln(1.166E/I)$, where $I = 11.5Z$ (eV).

Our goal is to solve Eq. (1) taking into account boundary condition (11), and to evaluate the distribution of backscattered electrons over angle and energy,

$$R(\theta,\phi,E) = |\cos\theta|N(\cos\theta,\phi,E,z=0) \quad \text{for} \quad \cos\theta<0. \tag{14}$$

This quantity after integration over angle and energy gives the total probability of backscattering,

$$R_{\rm tot} = [v_0\cos\theta_0]^{-1}\int_{-\pi}^{\pi}d\phi\int_{\pi/2}^{\pi}d\theta\sin\theta \times\int_0^{E_0}dE\,R(\theta,\phi,E), \tag{15}$$

where the normalization factor $[v_0\cos\theta_0]^{-1}$ is proportional to the flux associated with the incident beam. The magnitude of (15), as well as (14), depends on the mutual orientation of the incident beam and the crystal.

The kernel of Eq. (12) considered as an integral equation with respect to the variable ϕ is a convolution, since it depends on ϕ and ϕ' via the combination $\cos(\phi-\phi')$. This makes it possible to look for a solution of this equation in the form of the Fourier series

$$N(\cos\theta,\phi,E,z) = \frac{1}{2\pi}N(\cos\theta,0,E,z) + \frac{1}{\pi}\sum_{n=1}^{\infty}N(\cos\theta,n,E,z)\cos(n\phi). \tag{16}$$

In practice, the convergence of the series (16) depends on the angle of incidence, and for $\theta_0\sim 70°$ it is necessary to retain about 20 terms on the right-hand side of expression (16). Each Fourier component entering (16) satisfies a *separate* equation of the form

$$\mu\frac{\partial}{\partial z}N(\mu,n,E,z) = \int_{-1}^{1}d\mu'\,w_{\rm el}(\mu,\mu',n,E)N(\mu',n,E,z) + \frac{\partial}{\partial E}\left[\bar{\epsilon}(E)N(\mu,n,E,z)\right] - w_{\rm el}^{(\rm tot)}(E)N(\mu,n,E,z) + Q(\mu,n,E,z), \tag{17}$$

where μ denotes the cosines of the polar angle. Explicit expressions for $w_{\rm el}(\mu,\mu',n,E)$ and $Q(\mu,n,E,z)$ are given in Appendix B. The boundary condition on (17) is

$$N(\mu,n,E,z=0) = 0 \quad \text{for} \quad 0<\mu<1, \tag{18}$$

and we are interested in finding the quantities $N(\mu,n,E,z=0)$ in the region $-1<\mu<0$.

Taking into account that evaluation of experimental quantities requires integration over some finite ranges of angle

and energy, we define the function $N(\mu, n, E, z)$ on a grid of values of E and μ in the region $0 < E < E_0$ and $-1 < \mu < 1$, namely,

$$N_j^{(m)}(n,z) = \frac{1}{\Delta\mu}\int_{\mu_j-\Delta\mu/2}^{\mu_j+\Delta\mu/2} d\mu\, N(\mu, n, E_m, z), \tag{19}$$

and rewrite Eq. (17) in the matrix form

$$\mu_j \frac{\partial}{\partial z} N_j^{(m)}(n,z) = \Delta\mu \sum_{j'} w_{\rm el}^{jj'}(n, E_m) N_{j'}^{(m)}(n,z) - w_{\rm el}^{(\rm tot)}(E_m) N_j^{(m)}(n,z) + \frac{\bar{\epsilon}(E_{m-1})}{\Delta E} N_j^{(m-1)}(n,z) - \frac{\bar{\epsilon}(E_m)}{\Delta E} N_j^{(m)}(n,z) + Q_j^{(m)}(n,z), \tag{20}$$

where

$$w_{\rm el}^{jj'}(n, E_m) = \frac{1}{\Delta\mu}\int_{\mu_{j'}-\Delta\mu/2}^{\mu_{j'}+\Delta\mu/2} d\mu' w_{\rm el}(\mu_j, \mu', n, E_m) \tag{21}$$

and

$$Q_j^{(m)}(n,z) = \frac{1}{\Delta\mu}\int_{\mu_j-\Delta\mu/2}^{\mu_j+\Delta\mu/2} d\mu\, Q(\mu, n, E_m, z). \tag{22}$$

In solving Eq. (20) we will be following the method developed by Fathers and Rez,[31,32] although some of our definitions differ from those used in Refs. 31, 32 (Fathers and Rez considered a problem of solving a *homogeneous* transport equation for scattering of high-energy electrons in an amorphous solid). There is also a close similarity between the present method and an approach to the problem of deconvolution of energy loss spectra proposed for the transmission geometry of scattering by Schattschneider.[49] In the latter case the author developed a more advanced treatment which makes it possible to avoid using the continuous slowing down approximation adopted in Eq. (17).

We note that (20) has the form of a set of ordinary differential equations with constant coefficients, and so we can look for an appropriate solution of these equations in the form of a linear combination of eigenstates of the matrix describing coupling between various functions $N_j^{(m)}(n,z)$. We need to find the values of $N_j^{(m)}(n,0)$ corresponding to $\mu_j < 0$. In principle, these values can be readily determined if we notice that $N_j^{(m)}(n,0) = 0$ for $\mu_j > 0$, and take into account the condition that for a semi-infinite crystal there must be no terms diverging at $z = \infty$ (see Appendix C for more details). However, straightforward implementation of this principle is very demanding computationally and requires diagonalization of a very large matrix. Indeed, in order to achieve reasonable accuracy of computations, we need to take into account about $J_E \sim 20$ points approximating the energy spectrum and $J_\mu \sim 50$ points describing the angular distribution of electrons, therefore arriving at the problem of finding eigenvalues and eigenvectors of a large matrix of the order of 1000×1000 (some of our computational results presented below have been obtained using $J_E = 30$ and $J_\mu = 120$). In order to avoid the necessity of diagonalization of a large matrix, we employ the supermatrix algorithm.[31,32] The basic idea of the supermatrix approach consists in successive diagonalization of matrices $w_{\rm el}^{jj'}(n, E_0)$, $w_{\rm el}^{jj'}(n, E_1)$, $w_{\rm el}^{jj'}(n, E_2), \ldots$ followed by recursive computation of angular distributions of backscattered electrons at each point of the energy spectrum E_0, E_1, $E_2, \ldots$. This procedure is described in more detail in Appendix C. After all the quantities $N_j^{(m)}(n,0)$ have been calculated, the total coefficient of backscattering (15) can be found as

$$R_{\rm tot} = \frac{\Delta\mu\Delta E}{v_0 \cos\theta_0} \sum_{j,\ \mu_j<0} \sum_{m=1}^{J_E} |\mu_j| N_j^{(m)}(0,0). \tag{23}$$

A similar expression is valid for the distribution of backscattered electrons over angle and energy. Implementation of the supermatrix algorithm is relatively straightforward and, for instance, for $J_\mu = 48$ and $J_E = 10$ it takes only 15 s on a Hewlett-Packard Apollo workstation in order to calculate the entire distribution of backscattered electrons over angle and energy for a particular orientation of the incident beam.

IV. RESULTS AND DISCUSSION

We start with a verification of the reliability of the method based on the inhomogeneous transport equation (20). As an example we compare the values of the total coefficient of backscattering which have been calculated using the method described above, with experimental data and Monte Carlo simulations of electron backscattering from amorphous solids.[50] The results of this comparison are shown in Fig. 3. Generally our computational results agree well with the results of Monte Carlo simulations,[50] and both theoretical approaches are in an equally good correspondence with the experimental data. The deviation of the computed values from the experimental data is probably associated with the use of an approximate representation of the cross section of scattering by a single atom [Eq. (13)] (for a discussion of some other approximate representations see Ref. 51). In the present paper we do not attempt to improve the agreement for all the elements in Fig. 3, but instead we proceed to consider the electron backscattering from silicon single crystals, for which our method gives good

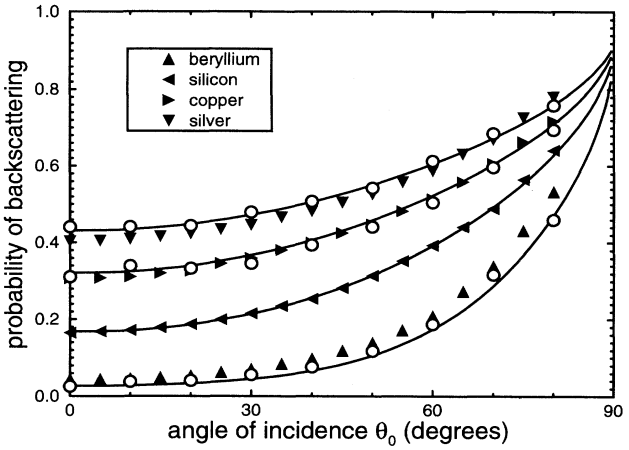

FIG. 3. The total probability of backscattering of electrons from amorphous materials measured experimentally and calculated theoretically as a function of the angle of incidence. The circles represent the results of Monte Carlo simulations of electron backscattering taken from Ref. 50, while the triangles are experimental results taken from the same source. The solid curves have been computed using the supermatrix algorithm described in the text for J_E =30 and J_μ =120. The energy of the electrons E_0 = 25 keV.

agreement with the experimental results (Fig. 3).

In order to evaluate the angular and energy distributions of electrons backscattered from a crystal, we transform the source function (8) in order to make it more amenable to numerical computations. First we notice that for large angles of scattering, many times the Bragg angle, the source function has the form

$$Q(\mathbf{n},E,\mathbf{r}) \approx v\left(\frac{m}{2\pi\hbar^2}\right)^2 \delta(E-E_0)\frac{1}{\Omega}\sum_\alpha\sum_{h,l}\phi_h(\mathbf{r})\phi_l^*(\mathbf{r}) \times|U_\alpha(\mathbf{k}_0-\mathbf{k})|^2\exp[-i(\mathbf{G}_l-\mathbf{G}_h)\cdot\mathbf{r}_\alpha] \times\exp[-M_\alpha(\mathbf{G}_l-\mathbf{G}_h)], \quad (24)$$

and that it behaves in a way which is similar to the behavior of the cross section of elastic scattering of fast electrons by a single atom α, namely,

$$\left(\frac{d\sigma_\alpha}{do}\right)_{\rm el} = \left(\frac{m}{2\pi\hbar^2}\right)^2 |U_\alpha(\mathbf{k}_0-\mathbf{k})|^2.$$

Therefore, the only difference between the angular distribution of electrons generated by the source function (24) and the angular distribution of electrons resulting from a single scattering in an amorphous substance is associated with the region of relatively small angles of scattering of the order of the Bragg angle. These angles correspond to a momentum transfer of the order of a reciprocal lattice vector ($|\mathbf{k}_0-\mathbf{k}| \sim |\mathbf{G}|$). Bearing in mind that we are considering plain geometry of scattering in which all the diffracted beams propagate downwards into the crystal, and taking into account the fact that the grazing angle of incidence ζ_0 (= 90° − θ_0) greatly exceeds the Bragg angle, we can neglect the details of the angular distribution generated by the source function (8) in the region $|\mathbf{k}_0-\mathbf{k}| \sim |\mathbf{G}|$ and rewrite this function $Q(\mathbf{n},E,\mathbf{r})$ in a form

$$Q(\mathbf{n},E,\mathbf{r}) = \delta(E-E_0+\bar{\epsilon}(E_0)z/\cos\theta_0)\frac{w_{\rm el}(\cos\psi_0,E_0)}{w_{\rm el}^{\rm (tot)}(E_0)}\frac{1}{\hbar} \times\sum_{h,l}\phi_h(z)\phi_l^*(z)\gamma_{lh}, \quad (25)$$

where θ_0 denotes the angle of incidence, $\cos\psi_0 = \sin\theta\sin\theta_0\cos(\phi-\phi_0)+\cos\theta\cos\theta_0$, and where we have taken into account the possibility of the electron losing energy before scattering through a relatively large angle. Note that the source function (25) satisfies the same condition (10) as the source function (8), being at the same time more suitable for expanding as a Fourier series (16). All the angular and energy distributions of electrons discussed below have been computed using this form of the source function (25).

We start by considering the energy spectrum of the backscattered electrons. The fact that the spectrum may exhibit a noticeable dependence on the orientation of the incident beam was shown experimentally by Wolf *et al.*[17] A similar effect for lower-energy electrons was demonstrated by Gomoyunova *et al.*[52] This dependence was analyzed theoretically by Sandström *et al.*[12] using the forward-backward (FB) approximation. In discussing the limitations of the FB approach, Sandström *et al.*[12] noted that the FB method does not take into account scattering through intermediate angles $\vartheta \sim 90°$, and as a result it does not predict the existence of a maximum of the energy spectrum. The reversal of channeling contrast when electrons with different energies are selected,[17] which is evident from the curves in Fig. 4, cannot be described

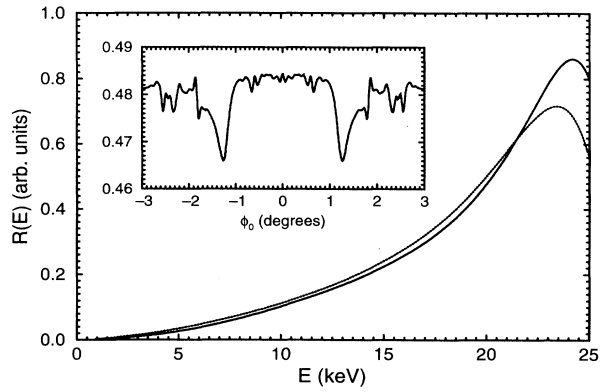

FIG. 4. Energy spectra $R(E) = \int_{-\pi}^{\pi}d\phi\int_{\pi/2}^{\pi}d\theta \sin\theta R(\theta,\phi,E)$ of electrons backscattered from single crystal of silicon. Solid curve corresponds to the spectrum evaluated for the direction of incidence θ_0 = 69° and ϕ_0 = 0.44°; the dotted curve corresponds to the direction θ_0 = 69° and ϕ_0 = 1.26°. The total probability of backscattering $R(\theta_0,\phi_0)$ plotted as a function of azimuthal angle of incidence ϕ_0 [ϕ_0 = 0 corresponds to the (220) planes of crystal lattice of silicon] for θ_0 = 69° and E_0 = 25 keV is shown in the inset. $R(\theta_0,\phi_0)$ is seen to fluctuate around the value $R(\theta_0)$ = 0.48, which is equal to the probability of backscattering for amorphous silicon.

by the FB approximation. In other words, if we compare the energy spectra of backscattered electrons, one corresponding to the direction of anomalous transmission ($\phi_0 = 1.26°$, dotted curve in Fig. 4) and the other corresponding to the direction of anomalous absorption of the electrons ($\phi_0 = 0.44°$, solid curve in Fig. 4), then the *shapes* of the energy spectra will differ for these two cases. Generally speaking, the peaks of the spectra behave in a similar way to the total probability of backscattering, which is shown in the inset in Fig. 4 as a function of the azimuthal angle of incidence ϕ_0 for $\theta_0 = 69°$. However, the behavior in the tails of the energy spectra is opposite to that near the peaks. A behavior of the energy spectra of the electrons similar to that shown in Fig. 4 was discovered experimentally by Wolf *et al.*[17] As follows from their results, the contrast of the channeling patterns observed using a particular type of a detector may depend noticeably on the response function $D(E)$ of the detector, and in some cases small changes in the response function may have a substantial influence on the magnitude of the contrast and can even result in a change of its sign. In what follows we will be discussing experimental observations carried out using two types of detectors, namely, a Si detector[15] and an yttrium aluminum garnet (YAG) detector.[1,2] Response functions of both types of detectors have a similar form[53]

$$D(E) = \frac{E - E_{\rm th}}{E_0 - E_{\rm th}}, \quad E > E_{\rm th}, \tag{26}$$

where $E_{\rm th}$ denotes the threshold energy (which is a quantity of the order of 2 keV for the YAG detector[53]), and E_0 is the energy of the incident beam. The observable signal can be represented as

$$I(\theta_0;\phi_0) = \int_{D[\phi]} d\phi \int_{D[\theta]} d\theta \sin\theta \times \int_{E_{\rm th}}^{E_0} dE\, D(E) R(\theta,\phi,E), \tag{27}$$

where the functions $D[\phi]$ and $D[\theta]$ determine the range of solid angles corresponding to the acceptance window of the detector. In (27) it is emphasized that for the case of electron backscattering from crystals, the signal depends both on the polar and azimuthal angles of scattering. Using (27), we can define the contrast as

$$C(\theta_0;\phi_0) = \frac{I(\theta_0;\phi_0) - I_{\rm am}(\theta_0)}{I_{\rm am}(\theta_0)}, \tag{28}$$

where $I_{\rm am}(\theta_0)$ corresponds to the intensity of backscattering from an amorphous solid.

As was noted above, the shape of the energy spectrum of electrons backscattered from a crystal is sensitive to the orientation of the incident beam, and this agrees with experimental observations.[17] Another interesting aspect of the problem of backscattering of electrons from crystals at oblique incidence has been investigated by Ichinokawa *et al.*,[15] who presented experimental evidence that the sign of the channeling contrast depends not only on the particular region of the energy spectrum chosen for observations, but also on the detector position (i.e., on the angles θ and ϕ). They found that the contrast is "normal" (i.e., the observed signal is lower if the direction of incidence coincides with a direction of anomalous transmission of electrons in the bulk crystal) for all angles of incidence provided that the detector is placed at a shallow take-off angle along the direction of the incident beam. However, if the detector is positioned to receive electrons scattered through relatively large angles ($\vartheta \sim 90°$), then inversion of the contrast may take place for grazing angles of incidence, ζ_0 ($\zeta_0 = 90° - \theta_0$), smaller than a particular critical angle ζ_c (the magnitude of which depends on the position of the detector). In Fig. 5 the dependence of the channeling contrast calculated for the (220) channeling band of Si on take-off angle χ ($= 180° - \theta$) is shown. Negative values of χ in Fig. 5 correspond to scattering towards the backward hemisphere $\phi = 180°$. As seen from the curves in Fig. 5, for $\theta_0 = 50°$ ($\zeta_0 = 40°$) the contrast is "normal" (positive) for all χ. However, with increasing angle of incidence there appears a large region of the take-off angles where the contrast is negative (for $\theta_0 = 65°$ this region lies between $\chi \approx -45°$ and $\chi \approx 47°$). In Figs. 6 and 7 electron channeling patterns calculated numerically for two different positions of the detector are shown. Figure 6 corresponds to the detector in the direction defined by $\chi = 80°$ and $\phi = 0°$, while for Fig. 7 the corresponding parameters are $\chi = 40°$ and $\phi = 180°$. These two directions coincide with those chosen by Ichinokawa *et al.*[15] for carrying out experimental observations. The (220) channeling band, the center of which coincides with the plane $\phi = 0°$, is clearly visible in both patterns. In the case of the low-angle detector position (Fig. 6) the contrast of the band remains normal over the entire range of the angles of incidence. For the high-angle detector position (Fig. 7) the contrast changes sign for grazing angles of incidence, ζ_0, smaller than $\zeta_c \sim 26°$. The intensity distributions shown in Figs. 6 and 7 are very similar to

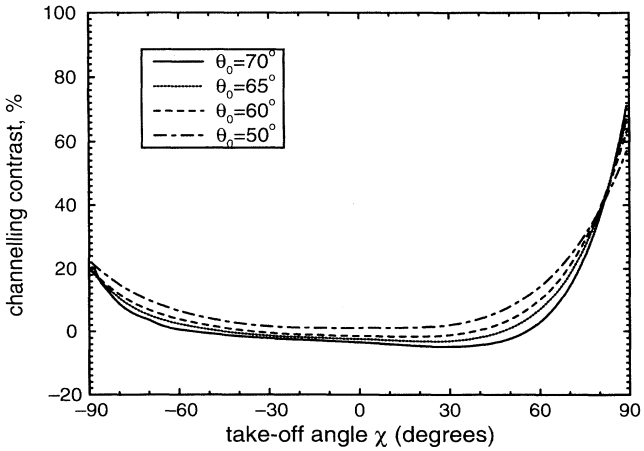

FIG. 5. The contrast of the Si (220) channeling band evaluated as a function of the take-off angle χ for $\phi \approx 0°$ ($\chi > 0$) and $\phi \approx 180°$ ($\chi < 0$) for various angles of incidence. The energy of the electrons $E_0 = 25$ keV, and computations have been performed using $J_\mu = 80$, $J_E = 15$.

the distributions shown in Figs. 3(a) and 3(b) of Ref. 15. The value of the critical angle ζ_c found experimentally ($\zeta_c = 22°$) appears to be somewhat lower than the value $\zeta_c = 26°$ found numerically, although it should be noted that this value is sensitive to the choice of the form of the response function of the detector [Eq. (26)] and to the magnitude of the screening parameter β in Eq. (13). Changes in E_{th} and β may result in a variation of ζ_c over a range of a few degrees.

Recent experimental studies[1,2] have demostrated that oblique incidence and low take-off angles are particularly suitable for observation of defects in crystals using the scanning electron microscope (SEM). Examination of the results presented in Figs. 5 and 6 shows that the magnitude of the channeling contrast increases rapidly with increase of the take-off angle (for $\chi > 0$), and is not particularly sensitive to the angle of incidence. Another quantity which determines the feasibility of carrying out experimental observations in SEM's is the signal-to-noise ratio (S/N). This is given by $\sqrt{n}$, where n is the number of electrons collected by the detector in the recording time. The contrast C of a channeling band should significantly exceed the inverse of this ratio if it is to be observable. The factor $C(\text{S/N}) > 5$ is often taken as a suitable criterion.[54] The actual signal-to-noise ratio depends on the detector window area and recording time, i.e., on the total number of electrons collected. However, for a given detector and recording time and for a fixed incident beam current, the factor above will scale with take-off angle χ as shown in Fig. 8. This shows the variation with χ of C multiplied by the square root of the scattered beam intensity, for the same set of angles of incidence as used for evaluation of the channeling contrast (Fig. 5). Negative values of the product evident over certain ranges of χ in Fig. 8 simply reflect a change of sign of the contrast C. The results shown in Fig. 8 demonstrate that while the channeling contrast itself depends rather weakly on the angle of incidence, the factor $C(\text{S/N})$ decreases rapidly with decreasing angle of incidence θ_0. This shows that both oblique incidence and a shallow-angle detector position are required in order to obtain both high contrast *and* high S/N ratio, in agreement with experimental observations.[1,2]

In this section we have described how application of the

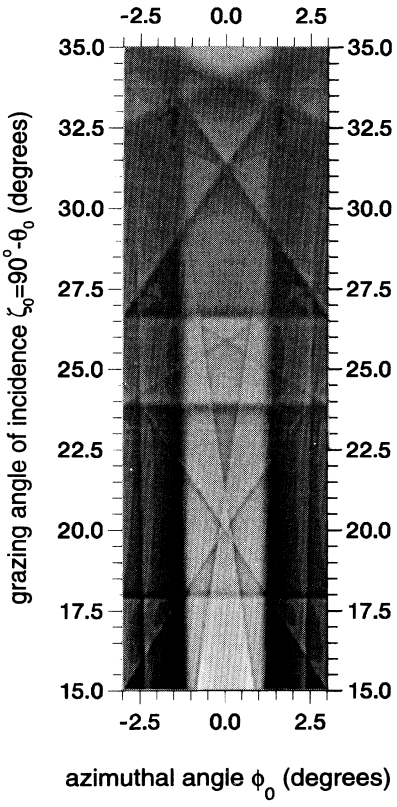

FIG. 6. The intensity distribution in the channeling pattern computed numerically for the (001) face of a single crystal of Si and for a low-angle position of the detector (Ref. 15), namely, $\zeta = 10°$ and $\phi = 0°$. The azimuth $\phi_0 = 0°$ is parallel to the (220) planes, and $E_0 = 25$ keV. Calculations have been performed using 14 terms of the expansion (16) and 26 functions $\phi_h(z)$ in (5), and $E_{\text{th}} = 6$ keV.

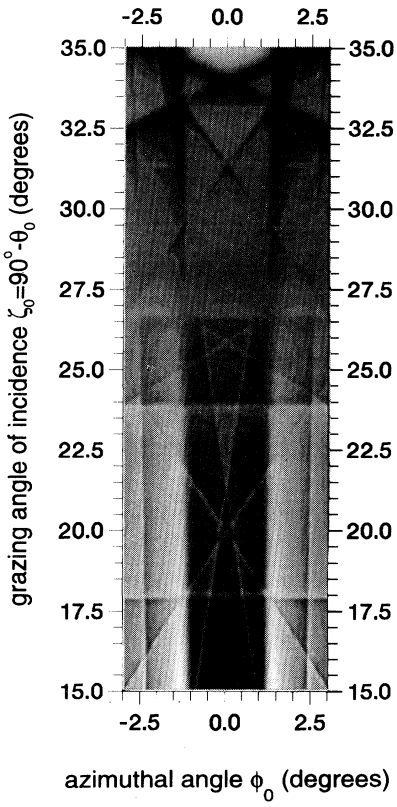

FIG. 7. Intensity distribution in the channeling pattern computed numerically for the (001) face of a single crystal of Si and for a high-angle position of the detector (Ref. 15), namely, $\zeta = 50°$ and $\phi = 180°$. The azimuth $\phi_0 = 0$ is parallel to the (220) planes, and $E_0 = 25$ keV. Calculations have been performed using 14 terms of the expansion (16) and 26 functions $\phi_h(z)$ in (5), and $E_{\text{th}} = 6$ keV. Note the effect of reversal of the contrast of the band at $\zeta_c \approx 26°$.

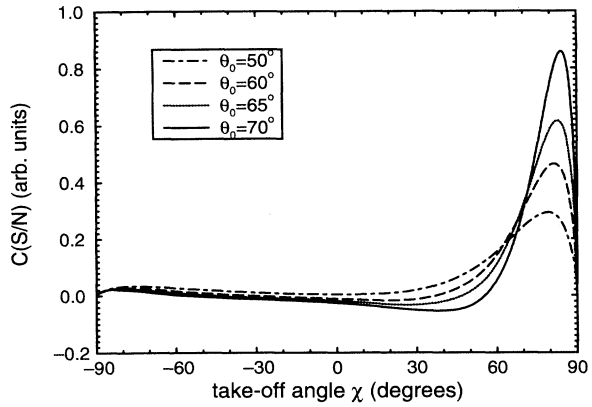

FIG. 8. The signal-to-noise ratio (see text for definition) for the Si (220) channeling band computed as a function of the take-off angle θ for $\phi \approx 0$ ($\chi > 0$) and $\phi \approx 180°$ ($\chi < 0$) for various angles of incidence. The energy of the electrons $E_0 = 25$ keV, and computations have been performed for $J_\mu = 80$, $J_E = 15$. Note the increase of the peak height with increasing angle of incidence.

full-scale multiple scattering approach to the problem of electron backscattering from crystals makes it possible to give a consistent interpretation to a number of phenomena which have been observed experimentally in the past and the origin of which have remained obscure so far. Nevertheless, the method used, which is based on a straightforward solution of the matrix equation (20), is relatively demanding computationally. In the following section we consider a perturbation expansion which in some cases can be employed for evaluation of the channeling contrast and which can considerably accelerate numerical computations.

V. PERTURBATION TREATMENT

In this section we derive an approximate expression for the channeling contrast, which is consistent with the multiple scattering treatment described above and which makes it possible to avoid the requirement of finding a numerical solution of Eq. (1) for each orientation of the incident beam. In the past this question was addressed by Howie,[13] who proposed that if one considers the background intensity as a phenomenological parameter known from experimental measurements, then it may be possible to develop a relatively simple scheme for calculating the magnitude of the *variation* of the backscattering signal. This idea was based on an argument that if the magnitude of the contrast is small (as a rule, this quantity is of the order of a few percent; see Fig. 4), then it may be possible to expand the exact solution in a series in which the zero-order term corresponds to the "averaged" background and the first-order term accounts for the contrast effects. In what follows we consider a series which satisfies this requirement and which provides a good approximation to the full-scale multiple scattering solution of the problem of electron backscattering.

Following the standard quantum-mechanical procedure for generating a perturbation expansion, we rewrite Eq. (12) in the integral form

$$N(\mu,\phi,E,z) = \int_0^\infty dz' \int_{-\pi}^{\pi} d\phi' \int_{-1}^{1} d\mu' \int_0^{E_0} dE' \mathcal{L}(\mu,\phi,E,z|\mu',\phi',E',z') Q(\mu',\phi',E',z'). \tag{29}$$

In this equation $\mathcal{L}(\mu,\phi,E,z|\mu',\phi',E',z')$ denotes the Green's function of the transport equation, i.e., a solution of Eq. (12) with a plane source situated at $z = z'$ and emitting electrons along a particular direction (θ',ϕ'), namely,

$$\begin{aligned}
&\mu \frac{\partial}{\partial z} \mathcal{L}(\mu,\phi,E,z|\mu',\phi',E',z') \\
&\quad = \int_{-\pi}^{\pi} d\phi'' \int_0^{\pi} d\theta'' \sin\theta'' w_{\mathrm{el}}(\cos\psi'',E) \mathcal{L}(\cos\theta'',\phi'',E,z|\mu',\phi',E',z') \\
&\qquad + \frac{\partial}{\partial E} [\bar{\epsilon}(E) \mathcal{L}(\mu,\phi,E,z|\mu',\phi',E',z')] - w_{\mathrm{el}}^{(\mathrm{tot})}(E) \mathcal{L}(\mu,\phi,E,z|\mu',\phi',E',z') \\
&\qquad + \delta(\mu-\mu')\delta(\phi-\phi')\delta(E-E')\delta(z-z'),
\end{aligned} \tag{30}$$

where $\mu' = \cos\theta'$.

Taking into account that the source located at $z' = 0$ is equivalent to a boundary condition, we find that the Green's function must obey the integral equation

$$\begin{aligned}
\mathcal{L}(\mu,\phi,E,0|\mu_0,\phi_0,E_0,0) &= \int_0^\infty dz' \int_{-\pi}^{\pi} d\phi' \int_{-1}^{1} d\mu' \int_0^{E_0} dE' \mathcal{L}(\mu,\phi,E,0|\mu',\phi',E',z') \\
&\quad \times w_{\mathrm{el}}(\cos\psi',E') \frac{1}{\bar{\epsilon}(E')} \delta\left(\frac{z'}{\mu_0} - \int_{E'}^{E_0} \frac{dE''}{\bar{\epsilon}(E'')} \right) \exp\left[-w_{\mathrm{el}}^{(\mathrm{tot})}(E') z'/\mu_0 \right] \\
&\approx \int_0^\infty dz' \int_{-\pi}^{\pi} d\phi' \int_{-1}^{1} d\mu' \mathcal{L}\left(\mu,\phi,E,0|\mu',\phi',E_0 - \bar{\epsilon}(E_0)\frac{z'}{\mu_0}, z' \right) \\
&\quad \times w_{\mathrm{el}}(\cos\psi',E_0) \exp[-w_{\mathrm{el}}^{(\mathrm{tot})}(E_0) z'/\mu_0].
\end{aligned} \tag{31}$$

In order to evaluate the *variation* of the intensity of backscattering associated with channeling of the incident electrons, we use formula (29) in which we substitute the *difference* between two source functions, the first one coinciding with (8) and the second one being the source function corresponding to an amorphous material,

$$\delta R(\mu,\phi,E) = |\cos\theta| \int_0^\infty dz' \int_{-\pi}^{\pi} d\phi' \int_{-1}^{1} d\mu' \mathcal{L}\left(\mu,\phi,E,0|\mu',\phi',E_0 - \frac{\bar{\epsilon}(E_0)z'}{\mu_0}, z'\right) \times \frac{w_{\rm el}(\cos\psi', E_0)}{w_{\rm el}^{\rm (tot)}(E_0)} \left[\frac{1}{\hbar}\sum_{h,l}\phi_h(z')\phi_l^*(z')\gamma_{lh} - v_0 w_{\rm el}^{\rm (tot)}(E_0)\exp[-w_{\rm el}^{\rm (tot)}(E_0)z'/\mu_0]\right]. \quad (32)$$

Expanding the Green's function under the integral sign as a Taylor series in z' and taking into account an equality which follows from (10),

$$\frac{1}{\hbar}\int_0^\infty dz \sum_{h,l}\phi_h(z)\phi_l^*(z)\gamma_{lh} = v_0\mu_0,$$

we find that the variation of backscattering intensity obeys a simple law

$$\delta R(\mu,\phi,E) = R(\mu,\phi,E) - R_{\rm rand}(\mu,\phi,E) = K(\mu,\phi,E|\mu_0,\phi_0,E_0) \times \int_0^\infty dz\, z \left[\frac{1}{\hbar}\sum_{h,l}\phi_h(z)\phi_l^*(z)\gamma_{lh} - v_0 w_{\rm el}^{\rm (tot)}(E_0)\exp[-w_{\rm el}^{\rm (tot)}(E_0)z/\mu_0]\right], \quad (33)$$

where the function $K(\mu,\phi,E|\mu_0,\phi_0,E_0)$ *does not* depend on the orientation of the crystal lattice and is proportional to the derivative of the Green's function of the transport equation with respect to the variable z, namely,

$$K(\mu,\phi,E|\mu_0,\phi_0,E_0) = |\cos\theta| \int_{-\pi}^{\pi} d\phi' \int_{-1}^{1} d\mu' \frac{w_{\rm el}(\cos\psi', E_0)}{w_{\rm el}^{\rm (tot)}(E_0)} \times \left(\frac{\partial}{\partial z'} - \frac{\bar{\epsilon}(E_0)}{\mu_0}\frac{\partial}{\partial E'}\right)\mathcal{L}(\mu,\phi,E,0|\mu',\phi',E',z')\Big|_{z'=0,\ E'=E_0}. \quad (34)$$

It should be emphasized that in practice in order to use the expansion (33), there is no need to find the Green's function and to calculate its derivative via (34). Evaluation of the two constants entering (33), $R_{\rm rand}(\mu,\phi,E)$ and $K(\mu,\phi,E|\mu_0,\phi_0,E_0)$, for a given pair of directions (θ_0,ϕ_0) and (θ,ϕ) can always be performed by fitting to the form (33) a numerical solution obtained using one adjustable parameter. As an example we substitute instead of the first term under the integral sign in (33) an expression which contains one free dimensionless parameter γ, namely, $Q(\mu,\phi,E,z) \sim v_0 w_{\rm el}^{\rm (tot)}(E_0)\gamma\exp[-w_{\rm el}^{\rm (tot)}(E_0)\gamma z/\mu_0]$, where γ varies between 0 and ∞. Qualitatively, the region $0 < \gamma < 1$ corresponds to anomalous transmission of electrons while the region $\gamma > 1$ can be attributed to anomalous absorption. Substituting this expression for the source function in (33) we find that within the range of validity of the perturbation expansion the intensity of backscattering follows the law

$$R(\mu,\phi,E) = C_0 + \frac{C_1}{\gamma}, \quad (35)$$

or, in other words, $R(\mu,\phi,E)$ varies linearly with γ^{-1}. The computational results shown in Fig. 9 and obtained using the full theory [Eq. (20)] demonstrate how the intensity of backscattering depends on γ^{-1} for various take-off angles. Generally in all the cases the intensity of backscattering varies almost linearly with γ^{-1}, and this confirms the validity of the perturbation expansion (33). The only case in which the dependence of backscattering intensity on γ^{-1} deviates from the linear law is the case of small take-off angle ζ, where the contrast can acquire values of the order of 100% (see Fig. 5). Therefore, we can see that over the entire range of the angles of incidence and backscattering there exists a perturbation expression for the channeling contrast, which does not contain any adjustable parameters and which makes it possible to evaluate the absolute value of the contrast by carrying out only a single integration over z. Expression (25) can be easily generalized to the case of imperfect crystals,[10,13] and this makes it possible to conclude that formula (33) represents a simple and suitable tool for carrying out computer simulations of channeling images of defects.

VI. CONCLUSIONS

In summary, in this paper we have developed a multiple scattering approach to the problem of electron backscattering from crystals and to the evaluation of the contrast of the channeling patterns. Numerical results obtained using this approach have made it possible to analyze in detail the dependence of angular distributions and energy spectra of backscattered electrons on the orientation of the incident beam, and to compare the results of com-

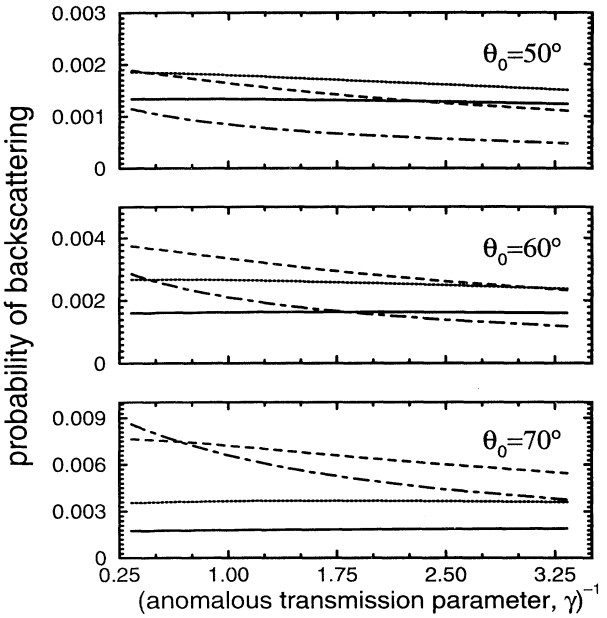

FIG. 9. The dependence of the differential probability of backscattering (i.e., the function $R_{\rm tot}^{(j)} = [\Delta\mu\Delta E/v_0\cos\theta_0]\sum_{m=1}^{J_E}|\mu_j|N_j^{(m)}(0,0))$ on the effective anomalous transmission parameter γ (see text) for various take-off angles. The linear dependence results from the first-order term of the perturbation expansion (33). The solid curve corresponds to $\chi = 30.40°$, the dotted curve to $\chi = 50.39°$, the dashed curve to $\chi = 70.28°$, and the dot-dashed curve to $\chi = 80.65°$. The energy of the electrons $E_0 = 25$ keV.

putations with experimental observations. We have generalized the perturbation approach proposed by Howie[13] and derived a simple expression which is consistent with the multiple scattering formulation of the problem and which is convenient for simulating channeling images of defects.

ACKNOWLEDGMENTS

We are grateful to Professor Sir Peter Hirsch, Professor A. Howie, and Dr. D. J. Dingley for stimulating discussions. We thank Dr. L.-M. Peng and Dr. J. T. Czernuszka for helpful discussions and comments regarding application of electron channeling to imaging of crystal defects. One of the authors (S.L.D.) acknowledges financial support of this work from the Engineering and Physical Science Research Counsil (EPSRC) (Grant No. GR/H96423). He is also grateful to Linacre College, Oxford, for financial support. Numerical computations have been performed using the facilities of the Materials Modelling Laboratory, Department of Materials, University of Oxford, which is funded in part by the EPSRC (Grant No. GR/H58278).

APPENDIX A

In this appendix we show how the transport equation (1) can be derived from the kinetic equation for the density matrix. The kinetic equation for $\rho(\mathbf{r},\mathbf{r}',E)$ has the form[29]

$$\rho(\mathbf{r},\mathbf{r}',E) = \rho_0(\mathbf{r},\mathbf{r}',E) + \int d^3x d^3x' G(\mathbf{r},\mathbf{x},E) \times G^*(\mathbf{r}',\mathbf{x}',E)\Big[\int d\omega\ \bar{s}(\mathbf{x}',\mathbf{x},\omega) \times\rho(\mathbf{x},\mathbf{x}',E+\hbar\omega)\Big], \tag{A1}$$

where $G(\mathbf{r},\mathbf{x},E)$ is the Green's function which describes propagation of the electron from $\mathbf{x}$ to $\mathbf{r}$. In Eq. (A1) the quantity $\rho_0(\mathbf{r},\mathbf{r}',E)$ represents the incident wave and associated elastic scattering, and the Green's function satisfies the equation

$$\Big[E+\frac{\hbar^2}{2m}\nabla^2 - \langle U(\mathbf{r})\rangle\Big]G(\mathbf{r},\mathbf{r}',E) - \int d^3x \int d\omega\ \bar{s}(\mathbf{r},\mathbf{x},\omega) G(\mathbf{r},\mathbf{x},E-\hbar\omega)G(\mathbf{x},\mathbf{r}',E) = \delta(\mathbf{r}-\mathbf{r}'). \tag{A2}$$

In Eqs. (A1) and (A2), $\langle U(\mathbf{r})\rangle$ denotes the part of the interaction which is averaged over the thermal ensemble and $\bar{s}(\mathbf{r},\mathbf{x},\omega)$ is the mixed dynamic form factor of inelastic excitations,[55]

$$\bar{s}(\mathbf{r},\mathbf{r}',\omega) = \frac{1}{\mathcal{Z}}\sum_{\nu,\nu'}\exp(-\epsilon_\nu/k_BT)\langle\nu|\delta U(\mathbf{r})|\nu'\rangle \times\langle\nu'|\delta U(\mathbf{r}')|\nu\rangle\delta\Big(\omega-\frac{\epsilon_{\nu'}-\epsilon_\nu}{\hbar}\Big), \tag{A3}$$

in which the matrix elements of the fluctuating part of the interaction $\langle\nu|\delta U(\mathbf{r})|\nu'\rangle$ are associated with inelastic transitions between various eigenstates of the medium.

Following Spencer and Humphreys,[24] we consider a two-stage mechanism of formation of the channeling patterns (see Fig. 2). The first stage involves diffraction of the incident electrons by the averaged potential $\langle U(\mathbf{r})\rangle$ and small-angle inelastic scattering by excitations of the electronic subsystem of the crystal (the term "small-angle scattering" corresponds to the case where the mean angle of scattering does not exceed the effective angular width of the Kikuchi lines). The second stage includes at least one event of scattering through a relatively large angle (in most cases this corresponds to phonon scattering) and subsequent propagation of the electron towards the surface. Formally we can represent the density matrix as a sum of two terms

$$\rho(\mathbf{r},\mathbf{r}',E) = \rho_{\rm SA}(\mathbf{r},\mathbf{r}',E) + \rho_{\rm LA}(\mathbf{r},\mathbf{r}',E), \tag{A4}$$

describing the electrons scattered through small and large angles, respectively. Considering the difference

$$\int d^3x G^{-1}(\mathbf{r},\mathbf{x},E)\rho(\mathbf{x},\mathbf{r}',E) - \int d^3x\rho(\mathbf{r},\mathbf{x},E)G^{-1}(\mathbf{x},\mathbf{r}',E),$$

and neglecting the influence of the averaged crystal po-

tential on propagation of electrons scattered through relatively large angles, we obtain the differential form of the kinetic equation,

$$\begin{aligned}\frac{\hbar^2}{2m}\ & (\nabla_{\mathbf{r}}^2-\nabla_{\mathbf{r}'}^2)\,\rho_{la}(\mathbf{r},\mathbf{r}',E)\\ &=\int d^3r''\int d\omega\ \bar{s}(\mathbf{r}-\mathbf{r}'',\omega)G(\mathbf{r}-\mathbf{r}'',E-\hbar\omega)\rho_{\mathrm{LA}}(\mathbf{r}'',\mathbf{r}',E)\\ &+\int d^3r'''\int d\omega\ \bar{s}(\mathbf{r}'''-\mathbf{r},\omega)G(\mathbf{r}'-\mathbf{r}''',E)\rho_{\mathrm{LA}}(\mathbf{r},\mathbf{r}''',E+\hbar\omega)\\ &-\int d^3r'''\int d\omega\ \bar{s}(\mathbf{r}'''-\mathbf{r}',\omega)G(\mathbf{r}'-\mathbf{r}''',E-\hbar\omega)\rho_{\mathrm{LA}}(\mathbf{r},\mathbf{r}''',E)\\ &-\int d^3r''\int d\omega\ \bar{s}(\mathbf{r}'-\mathbf{r}'',\omega)G(\mathbf{r}-\mathbf{r}'',E)\rho_{\mathrm{LA}}(\mathbf{r}'',\mathbf{r}',E+\hbar\omega)\\ &+\int d^3r'''\int d\omega\ \bar{s}(\mathbf{r}''',\mathbf{r},\omega)G(\mathbf{r}',\mathbf{r}''',E)\rho_{\mathrm{SA}}(\mathbf{r},\mathbf{r}''',E+\hbar\omega)\\ &-\int d^3r''\int d\omega\ \bar{s}(\mathbf{r}',\mathbf{r}'',\omega)G(\mathbf{r},\mathbf{r}'',E)\rho_{\mathrm{SA}}(\mathbf{r}'',\mathbf{r}',E+\hbar\omega),\end{aligned}\tag{A5}$$

where we have taken into account that for the electrons scattered through relatively large angles both the dynamic form factor and the Green's function can be represented in a form corresponding to a "random" orientation of the crystal lattice.[24,47] Representing $\rho_{\mathrm{LA}}(\mathbf{r},\mathbf{r}',E)$ as a linear combination of plane waves with slowly varying amplitudes,

$$\rho_{\mathrm{LA}}(\mathbf{r},\mathbf{r}',E)=\int\int\frac{d^3kd^3k'}{(2\pi)^6}W(\mathbf{k},\mathbf{k}',\mathbf{r},\mathbf{r}',E)\exp(i\mathbf{k}\cdot\mathbf{r}-i\mathbf{k}'\cdot\mathbf{r}'),\tag{A6}$$

and substituting (A6) into (A5), we can derive an equation for the diagonal elements $W(\mathbf{k},\mathbf{r},E)=W(\mathbf{k},\mathbf{k},\mathbf{r},\mathbf{r},E)$ of the amplitude function,

$$\begin{aligned}\frac{\hbar^2}{m}\mathbf{k}\frac{\partial}{\partial\mathbf{r}}W(\mathbf{k},\mathbf{r},E)=&\,\delta\left(E-\frac{\hbar^2\mathbf{k}^2}{2m}\right)\int\frac{d^3q}{(2\pi)^2}\int d\omega\bar{s}(\mathbf{q}-\mathbf{k},\omega)W(\mathbf{q},\mathbf{r},E+\hbar\omega)\\ &-\int\frac{d^3q}{(2\pi)^2}\int d\omega\bar{s}(\mathbf{k}-\mathbf{q},\omega)\delta\left(E-\hbar\omega-\frac{\hbar^2\mathbf{q}^2}{2m}\right)W(\mathbf{k},\mathbf{r},E)\\ &+2\pi\delta\left(E-\frac{\hbar^2\mathbf{k}^2}{2m}\right)\int_{|\mathbf{r}-\mathbf{x}|,|\mathbf{r}-\mathbf{x}'|\sim r_0}d^3xd^3x'\exp(-i\mathbf{k}\cdot\mathbf{x}+i\mathbf{k}\cdot\mathbf{x}')\\ &\times\int d\omega\bar{s}(\mathbf{x}',\mathbf{x},\omega)\rho_{\mathrm{SA}}(\mathbf{x},\mathbf{x}',E+\hbar\omega),\end{aligned}\tag{A7}$$

in which the value of r_0 is so chosen to satisfy the inequalities $r_{\mathrm{corr}}\ll r_0\ll l_W$, where r_{corr} is a characteristic distance between two arguments $\mathbf{x}$ and $\mathbf{x}'$ of the mixed dynamic form factor $\bar{s}(\mathbf{x}',\mathbf{x},\omega)$ determining the effective range over which this factor is appreciable, and the value of l_W characterizes the rate of variation of the function $W(\mathbf{k},\mathbf{r},E)$ in real space. Using the definition

$$F(\mathbf{n},E,\mathbf{r})=\int_0^\infty\frac{k^2dk}{(2\pi)^3}W(k\mathbf{n},\mathbf{r},E),\tag{A8}$$

Eq. (A7) can be transformed to the form (1).

APPENDIX B

Substituting the Fourier expansion (16) in the right-hand side of Eq. (12), we arrive at Eq. (17), where the coefficients $w_{\mathrm{el}}(\mu,\mu',n,E)$ and $Q(\mu,n,E,z)$ are defined as

$$w_{\mathrm{el}}(\cos\theta,\cos\theta',n,E)=\int_{-\pi}^{\pi}d\phi\ w_{\mathrm{el}}(\cos\psi,E)\cos(n\phi)\tag{B1}$$

and

$$Q(\cos\theta,n,E,z)=\int_{-\pi}^{\pi}d\phi\ Q(\cos\theta,\cos\phi,E,z)\cos(n\phi),\tag{B2}$$

where

$$\cos\psi = \sin\theta \sin\theta' \cos\phi + \cos\theta \cos\theta',$$

and $w_{\rm el}(\mu, \mu', n, E)$ and $Q(\mu, n, E, z)$ are given by expressions (13) and (25), respectively. Using the formula

$$\int_{-\pi}^{\pi} dx \frac{\cos(nx)}{(a + b\cos x)^2} = \frac{2\pi}{a^2 - b^2} \left\{ \frac{a}{\sqrt{a^2 - b^2}} + n \right\} \left[\frac{\sqrt{a^2 - b^2} - a}{b} \right]^n, \tag{B3}$$

we obtain

$$w_{\rm el}(\mu, \mu', n, E) = 2\pi n_V \left(\frac{Ze^2}{2E} \right)^2 \left[\frac{\dfrac{1 + \beta - \mu\mu'}{\sqrt{(1 + \beta - \mu\mu')^2 - (1 - \mu^2)(1 - \mu'^2)}} + n}{(1 + \beta - \mu\mu')^2 - (1 - \mu^2)(1 - \mu'^2)} \right]$$

$$\times \left[\frac{(1 + \beta - \mu\mu') - \sqrt{(1 + \beta - \mu\mu')^2 - (1 - \mu^2)(1 - \mu'^2)}}{\sqrt{(1 - \mu^2)(1 - \mu'^2)}} \right]^n \tag{B4}$$

and

$$Q(\mu, n, E, z) = \delta(E - E_0 + \bar{\epsilon}(E_0) z/\mu_0) \left\{ \sum_{h,l} \phi_h(z) \phi_l^*(z) \gamma_{lh} \right\}$$

$$\times \left[\frac{\beta(2 + \beta)}{2\hbar} \right] \left[\frac{\dfrac{1 + \beta - \mu_0\mu}{\sqrt{(1 + \beta - \mu_0\mu)^2 - (1 - \mu_0^2)(1 - \mu^2)}} + n}{(1 + \beta - \mu_0\mu)^2 - (1 - \mu_0^2)(1 - \mu^2)} \right]$$

$$\times \left[\frac{(1 + \beta - \mu_0\mu) - \sqrt{(1 + \beta - \mu_0\mu)^2 - (1 - \mu_0^2)(1 - \mu^2)}}{\sqrt{(1 - \mu_0^2)(1 - \mu^2)}} \right]^n. \tag{B5}$$

APPENDIX C

Introducing a generalized index $\alpha = (m, j, n)$, we can rewrite Eq. (20) in the form

$$\frac{d}{dz} N_\alpha(z) = \sum_\beta \Pi_{\alpha\beta} N_\beta(z) + Q_\alpha(z). \tag{C1}$$

Defining the matrix of eigenvectors $X_{\beta\gamma}$ and a set of eigenvalues p_γ of the matrix $\Pi_{\alpha\beta}$ as

$$\sum_\beta \Pi_{\alpha\beta} X_{\beta\gamma} = X_{\alpha\gamma} p_\gamma, \tag{C2}$$

we can obtain a solution of Eq. (C1) in the form

$$N_\alpha(z) = \sum_\beta X_{\alpha\beta} C_\beta(z) \exp(p_\beta z). \tag{C3}$$

Substituting (C3) into (C1), we arrive at

$$\frac{d}{dz} C_\beta(z) = \sum_\alpha (\hat{X}^{-1})_{\beta\alpha} Q_\alpha(z) \exp(-p_\beta z), \tag{C4}$$

integration of which from 0 to ∞ gives

$$C_\beta(\infty) - C_\beta(0) = \sum_\alpha (\hat{X}^{-1})_{\beta\alpha} \int_0^\infty Q_\alpha(z) \exp(-p_\beta z) dz. \tag{C5}$$

Taking into account that in the expansion (C3) there must be no terms diverging at $z = \infty$, we find

$$C_\beta(0) = -\sum_\alpha (\hat{X}^{-1})_{\beta\alpha} \int_0^\infty Q_\alpha(z) \exp(-p_\beta z) dz \tag{C6}$$

for all coefficients $C_\beta(0)$ corresponding to positive p_β. Equation (C6) represents $J_E \times J_\mu/2$ conditions on $J_E \times J_\mu$ coefficients $C_\beta(0)$. Some further $J_E \times J_\mu/2$ conditions follow from the equation

$$N_\alpha(0) = \sum_\beta X_{\alpha\beta} C_\beta(0) = 0, \tag{C7}$$

which must be satisfied for all α corresponding to $\mu_\alpha > 0$. After all the $J_E \times J_\mu$ coefficients $C_\beta(0)$ have been found, Eq. (C7) can be employed for evaluation of the distribution of backscattered electrons $N_\alpha(0)$ for $\mu_\alpha < 0$. The main step in realization of the algorithm outlined above consists in finding the matrices $\hat{X}$ and $\hat{X}^{-1}$ and the eigenvector $\{p\}$, avoiding carrying out straightforward numerical diagonalization of $\hat{\Pi}$.

Following Fathers and Rez[31,32] and taking into account that electrons can only lose energy, we can represent the matrix $\hat{\Pi}$ in the form

$$\begin{pmatrix} \hat{\Pi}^{(00)} & 0 & 0 & 0 & \dots \\ \hat{\Pi}^{(10)} & \hat{\Pi}^{(11)} & 0 & 0 & \dots \\ 0 & \hat{\Pi}^{(21)} & \hat{\Pi}^{(22)} & 0 & \dots \\ 0 & 0 & \hat{\Pi}^{(32)} & \hat{\Pi}^{(33)} & \dots \\ 0 & 0 & 0 & \hat{\Pi}^{(43)} & \dots \\ \dots & \dots & \dots & \dots & \dots \end{pmatrix},$$

where the submatrices $\hat{\Pi}^{(ii)}$ describe elastic scattering of electrons in the the energy level E_i, and the submatrices $\hat{\Pi}^{(i+1,i)}$ represent the probabilities of inelastic transitions between the energy levels E_i and E_{i+1}. It is evident that the matrix of eigenvectors has a triangular form

$$\begin{pmatrix} \hat{X}^{(00)} & 0 & 0 & 0 & \dots \\ \hat{X}^{(10)} & \hat{X}^{(11)} & 0 & 0 & \dots \\ \hat{X}^{(20)} & \hat{X}^{(21)} & \hat{X}^{(22)} & 0 & \dots \\ \hat{X}^{(30)} & \hat{X}^{(31)} & \hat{X}^{(32)} & \hat{X}^{(33)} & \dots \\ \hat{X}^{(40)} & \hat{X}^{(41)} & \hat{X}^{(42)} & \hat{X}^{(43)} & \dots \\ \dots & \dots & \dots & \dots & \dots \end{pmatrix}$$

and can be represented in a form of a product

$$\begin{pmatrix} \hat{X}^{(00)} & 0 & 0 & 0 & \dots \\ \hat{X}^{(10)} & \hat{X}^{(11)} & 0 & 0 & \dots \\ \hat{X}^{(20)} & \hat{X}^{(21)} & \hat{X}^{(22)} & 0 & \dots \\ \hat{X}^{(30)} & \hat{X}^{(31)} & \hat{X}^{(32)} & \hat{X}^{(33)} & \dots \\ \hat{X}^{(40)} & \hat{X}^{(41)} & \hat{X}^{(42)} & \hat{X}^{(43)} & \dots \\ \dots & \dots & \dots & \dots & \dots \end{pmatrix} = \begin{pmatrix} \hat{E} & 0 & 0 & 0 & \dots \\ \hat{T}^{(10)} & \hat{E} & 0 & 0 & \dots \\ \hat{T}^{(20)} & \hat{T}^{(21)} & \hat{E} & 0 & \dots \\ \hat{T}^{(30)} & \hat{T}^{(31)} & \hat{T}^{(32)} & \hat{E} & \dots \\ \hat{T}^{(40)} & \hat{T}^{(41)} & \hat{T}^{(42)} & \hat{T}^{(43)} & \dots \\ \dots & \dots & \dots & \dots & \dots \end{pmatrix} \begin{pmatrix} \hat{U}^{(00)} & 0 & 0 & 0 & \dots \\ 0 & \hat{U}^{(11)} & 0 & 0 & \dots \\ 0 & 0 & \hat{U}^{(22)} & 0 & \dots \\ 0 & 0 & 0 & \hat{U}^{(33)} & \dots \\ 0 & 0 & 0 & 0 & \hat{U}^{(44)} \\ \dots & \dots & \dots & \dots & \dots \end{pmatrix}, \tag{C8}$$

where $\hat{E}$ denotes the unit matrix and the submatrices $\hat{T}^{(ij)}$ are chosen in such a way to reduce the entire matrix $\hat{\Pi}$ to the block-diagonal form

$$\begin{pmatrix} \hat{\Pi}^{(00)} & 0 & 0 & 0 & \dots \\ \hat{\Pi}^{(10)} & \hat{\Pi}^{(11)} & 0 & 0 & \dots \\ 0 & \hat{\Pi}^{(21)} & \hat{\Pi}^{(22)} & 0 & \dots \\ 0 & 0 & \hat{\Pi}^{(32)} & \hat{\Pi}^{(33)} & \dots \\ 0 & 0 & 0 & \hat{\Pi}^{(43)} & \dots \\ \dots & \dots & \dots & \dots & \dots \end{pmatrix} \begin{pmatrix} \hat{E} & 0 & 0 & 0 & \dots \\ \hat{T}^{(10)} & \hat{E} & 0 & 0 & \dots \\ \hat{T}^{(20)} & \hat{T}^{(21)} & \hat{E} & 0 & \dots \\ \hat{T}^{(30)} & \hat{T}^{(31)} & \hat{T}^{(32)} & \hat{E} & \dots \\ \hat{T}^{(40)} & \hat{T}^{(41)} & \hat{T}^{(42)} & \hat{T}^{(43)} & \dots \\ \dots & \dots & \dots & \dots & \dots \end{pmatrix}$$

$$= \begin{pmatrix} \hat{E} & 0 & 0 & 0 & \dots \\ \hat{T}^{(10)} & \hat{E} & 0 & 0 & \dots \\ \hat{T}^{(20)} & \hat{T}^{(21)} & \hat{E} & 0 & \dots \\ \hat{T}^{(30)} & \hat{T}^{(31)} & \hat{T}^{(32)} & \hat{E} & \dots \\ \hat{T}^{(40)} & \hat{T}^{(41)} & \hat{T}^{(42)} & \hat{T}^{(43)} & \dots \\ \dots & \dots & \dots & \dots & \dots \end{pmatrix} \begin{pmatrix} \hat{\Pi}^{(00)} & 0 & 0 & 0 & \dots \\ 0 & \hat{\Pi}^{(11)} & 0 & 0 & \dots \\ 0 & 0 & \hat{\Pi}^{(22)} & 0 & \dots \\ 0 & 0 & 0 & \hat{\Pi}^{(33)} & \dots \\ 0 & 0 & 0 & 0 & \dots \\ \dots & \dots & \dots & \dots & \dots \end{pmatrix}, \tag{C9}$$

and each of the matrices $\hat{U}^{(ii)}$ is a matrix of eigenvectors of $\hat{\Pi}^{(ii)}$. Performing multiplication in (C9), we arrive at a system of commutatorlike equations,

$$\begin{aligned} \hat{\Pi}^{(10)} + \hat{\Pi}^{(11)}\hat{T}^{(10)} &= \hat{T}^{(10)}\hat{\Pi}^{(00)}, \\ \hat{\Pi}^{(21)}\hat{T}^{(10)} + \hat{\Pi}^{(22)}\hat{T}^{(20)} &= \hat{T}^{(20)}\hat{\Pi}^{(00)}, \\ \hat{\Pi}^{(21)}\hat{T}^{(11)} + \hat{\Pi}^{(22)}\hat{T}^{(21)} &= \hat{T}^{(21)}\hat{\Pi}^{(11)}, \\ &\dots, \end{aligned} \tag{C10}$$

by solving which we can find the matrices $\hat{T}^{(10)}$, $\hat{T}^{(20)}$, $\hat{T}^{(21)}$ etc.

A similar recurrence procedure can be used for evaluation of the inverse matrix $\hat{X}^{-1}$. Representing $\hat{X}$ in the form $\hat{X} = \hat{T}\hat{U}$, where $\hat{U}$ is a block-diagonal matrix introduced in (C8), we obtain $\hat{X}^{-1} = \hat{U}^{-1}\hat{T}^{-1}$. Using the notation $\hat{T}^{-1} = \hat{R}$, and taking into account the fact that $\hat{R}$ is a triangular matrix, all the above-diagonal blocks of which are equal to zero, we arrive at a sequence of recurrence relations,

$$\begin{aligned} \hat{R}^{(00)} &= \hat{E}, \\ \hat{T}^{(10)}\hat{R}^{(00)} + \hat{R}^{(10)} &= 0, \\ \hat{T}^{(20)}\hat{R}^{(00)} + \hat{T}^{(21)}\hat{R}^{(10)} + \hat{R}^{(20)} &= 0, \\ &\dots \\ \hat{R}^{(11)} &= \hat{E}, \\ \hat{T}^{(21)}\hat{R}^{(11)} + \hat{R}^{(21)} &= 0, \\ \hat{T}^{(31)}\hat{R}^{(11)} + \hat{T}^{(32)}\hat{R}^{(21)} + \hat{R}^{(31)} &= 0, \\ &\dots, \end{aligned} \tag{C11}$$

from which we can find all the blocks of the inverse matrix $\hat{T}^{-1}$, and subsequently the entire matrix $\hat{X}^{-1}$.

[1]J. T. Czernuszka, N. J. Long, E. D. Boyes, and P. B. Hirsch, Philos. Mag. Lett. **62**, 227 (1990).
[2]A. J. Wilkinson, G. R. Anstis, J. T. Czernuszka, N. J. Long, and P. B. Hirsch, Philos. Mag. A **68**, 59 (1993).
[3]G. R. Booker, A. M. B. Shaw, M. J. Whelan, and P. B. Hirsch, Philos. Mag. **16**, 1185 (1967).
[4]D. G. Coates, Philos. Mag. **16**, 1179 (1967).
[5]D. C. Joy, D. E. Newbury, and D. L. Davidson, J. Appl. Phys. **53**, R81 (1982); D. C. Joy, Ultramicroscopy **37**, 216 (1991).
[6]P. Morin, M. Pitaval, D. Besnard, and G. Fontain, Philos. Mag. **40**, 511 (1979).
[7]P. B. Hirsch and C. J. Humphreys, in *Scanning Electron Microscopy 1970*, edited by O. Johari (IIT Research Institute, Chicago, 1970), p. 451.
[8]E. Vicario, M. Pitaval, and G. Fontaine, in *Microscopie Électronique 1970*, edited by P. Favard (Soc. Franc. Micr. Electron., Paris, 1970), Vol. II, p. 211.
[9]L. Reimer, H. G. Badde, and H. Seidel, Z. Angew. Phys. **31**, 145 (1971).
[10]D. R. Clarke and A. Howie, Philos. Mag. **24**, 959 (1971).
[11]J. P. Spencer, C. J. Humphreys, and P. B. Hirsch, Philos. Mag. **26**, 193 (1972).
[12]R. Sandström, J. F. Spencer, and C. J. Humphreys, J. Phys. D **7**, 1030 (1974).
[13]A. Howie, in *Quantitative Scanning Electron Microscopy*, edited by D. B. Holt, M. D. Muir, P. R. Grant, and I. M. Boswarva (Academic Press, London, 1974), p. 183.
[14]K. Marthinsen and R. Høier, Acta Crystallogr. A **42**, 484 (1986); **44**, 693 (1988); **44**, 700 (1988); K. Marthinsen, Dr. Ing. thesis, Universitetet i Trondheim, 1986.
[15]T. Ichinokawa, M. Nishimura, and H. Wada, J. Phys. Soc. Jpn. **36**, 221 (1974).
[16]T. Yamamoto, M. Mori, and Y. Ishida, Philos. Mag. **38**, 439 (1978).
[17]E. D. Wolf, P. J. Coane, and T. E. Everhart, in *Microscopie Électronique 1970* (Ref. 8), Vol. II, p. 595.
[18]T. Matsukawa, R. Shimizu, and H. Hashimoto, J. Appl. Phys. **7**, 695 (1974).
[19]H. Niedrig, J. Appl. Phys. **53**, R15 (1982).
[20]G. R. Massoumi, N. Hozhabri, K. O. Jensen, W. N. Lennard, M. S. Lorenzo, P. J. Schultz, and A. B. Walker, Phys. Rev. Lett. **68**, 3873 (1992).
[21]H. Drescher, E. R. Kreifting, L. Reimer, and H. Seidel, Z. Naturforsch. Teil A **29**, 833 (1974).
[22]P. Morin, Ph.D. thesis, Université de Lyon, 1981.
[23]G. Fontain, P. Morin, and M. Pitaval, in *Microscopy of Semiconducting Materials*, Proceedings of the Institute of Physics Conference, Oxford, 1983, edited by A. G. Cullis, S. M. Davidson, and G. R. Booker, IOP Conf. Proc. No. 67 (Institute of Physics, Bristol, 1983), p. 213.
[24]J. P. Spencer and C. J. Humphreys, Philos. Mag. **42**, 433 (1980).
[25]Yu. Kagan and Yu. V. Kononets, Zh. Eksp. Teor. Fiz. **64**, 1042 (1973) [Sov. Phys. JETP **37**, 530 (1973)].
[26]P. Rez, in *Electron Diffraction 1927-1977*, Proceedings of the International Conference on Electron Diffraction, edited by P. J. Dobson, J. B. Pendry, and C. J. Humphreys, IOP Conf. Proc. No. 41 (Institute of Physics and Physical Society, Bristol, 1978), p. 61.
[27]S. L. Dudarev, L.-M. Peng, and M. J. Whelan, Phys. Lett. A **170**, 111 (1992); **175**, 465 (1993).
[28]L.-M. Peng, S. L. Dudarev, and M. J. Whelan, Phys. Lett. A **175**, 461 (1993).
[29]S. L. Dudarev, L.-M. Peng, and M. J. Whelan, Phys. Rev. B **50**, 14525 (1994).
[30]S. L. Dudarev, D. D. Vvedensky, and M. J. Whelan, Phys. Rev. B **50**, 14525 (1994).
[31]D. J. Fathers and P. Rez, *Scanning Electron Microscopy, 1979, Part I* (SEM Inc., AMF O'Hare, IL 60666), p. 55.
[32]D. J. Fathers and P. Rez, in *Electron Beam Interactions with Solids*, edited by D. F. Kyzer, H. Niedrig, D. E. Newbury, and R. Shimizu (SEM Inc., AMF O'Hare, IL, 1984), p. 193.
[33]J. A. Venables and C. J. Harland, Philos. Mag. **27**, 2293 (1973).
[34]K. Z. Baba-Kishi, Ultramicroscopy **34**, 205 (1990).
[35]D. J. Dingley and V. Randle, J. Mater. Sci. **27**, 4545 (1992).
[36]W. S. M. Werner, I. S. Tilinin, and M. Hayek, Phys. Rev. B **50**, 4819 (1994).
[37]S. L. Dudarev, L.-M. Peng, and M. J. Whelan, Proc. R. Soc. London A **440**, 567 (1993).
[38]P. B. Hirsch, A. Howie, R. B. Nicholson, D. W. Pashley, and M. J. Whelan, *Electron Microscopy of Thin Crystals* (Butterworths, London, 1965).
[39]D. Bird and Q. A. King, Acta Crystallogr. A **46**, 202 (1990).
[40]R. F. Dashen, Phys. Rev. **134**, A1025 (1964).
[41]N. P. Kalashnikov, V. S. Remizovich, and M. I. Ryazanov, *Collisions of Fast Charged Particles in Solids* (Atomizdat, Moscow, 1980).
[42]I. S. Tilinin, Zh. Eksp. Teor. Fiz. **82**, 1291 (1982) [Sov. Phys. JETP **55**, 751 (1982)].
[43]V. V. Grebenshchikov, S. S. Kozlovskii, Yu. S. Korobochko, V. I. Mineev, and A. F. Petrochenko, Pis'ma Zh. Tech. Fiz. **14**, 447 (1988) [Sov. Tech. Phys. Lett. **14**, 200 (1988)].
[44]L. D. Landau and E. M. Lifshitz, *Quantum Mechanics, Non-Relativistic Theory*, 3rd ed. (Pergamon Press, Oxford, 1977).
[45]M. J. Whelan, J. Appl. Phys. **36**, 2099 (1965); **36**, 2103 (1965).
[46]C. R. Hall and P. B. Hirsch, Proc. R. Soc. London A **286**, 158 (1965).
[47]S. L. Dudarev and M. J. Whelan, Surf. Sci. **311**, L687 (1994).
[48]V. B. Berestetskii, E. M. Lifshits, and L. P. Pitaevskii, *Quantum Electrodynamics*, 2nd ed. (Pergamon Press, Oxford, 1982).
[49]P. Schattschneider, Philos. Mag. B **47**, 555 (1983).
[50]H. Drescher, L. Reimer, and H. Seidel, Z. Angew. Phys. **29**, 331 (1970).
[51]P. Rez, in *Electron Beam Interactions with Solids* (Ref. 32), p. 43.
[52]M. V. Gomoyunova, S. L. Zaslavskij, and I. I. Pronin, Fiz. Tverd. Tela (Leningrad) **20**, 3645 (1978) [Sov. Phys. Solid State **20**, 2106 (1978)]; **24**, 390 (1982) [**24**, 221 (1982)].
[53]R. Autrata, P. Schauer, Jos. Kvapil, and J. Kvapil, *Scanning Electron Microscopy, 1983, Part II* (SEM Inc., AMF O'Hare, IL 60666), p. 489.
[54]G. R. Booker, in *Modern Diffraction and Imaging Techniques in Materials Science*, edited by S. Amelinckx, R. Gevers, G. Remault, and J. Van Landuyt (North-Holland, Amsterdam, 1970), p. 569.
[55]H. Kohl and H. Rose, in *Advances in Electronics and Electron Physics*, edited by P. W. Hawkes (Academic Press, Orlando, 1985), Vol. 65, p. 173.

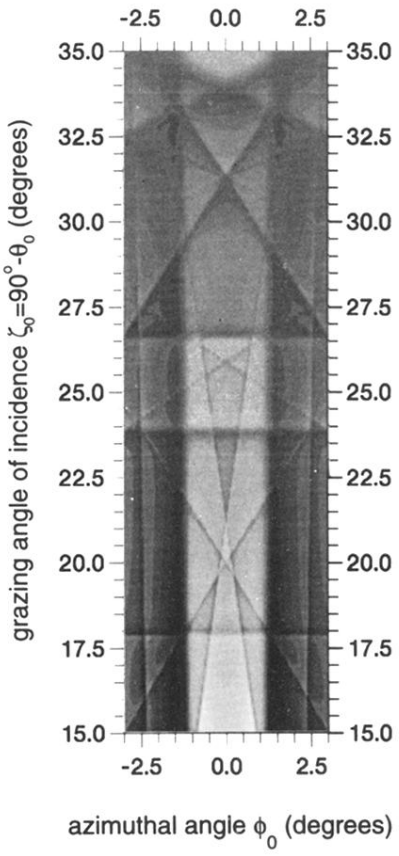

FIG. 6. The intensity distribution in the channeling pattern computed numerically for the (001) face of a single crystal of Si and for a low-angle position of the detector (Ref. 15), namely, $\zeta = 10°$ and $\phi = 0°$. The azimuth $\phi_0 = 0°$ is parallel to the (220) planes, and $E_0 = 25$ keV. Calculations have been performed using 14 terms of the expansion (16) and 26 functions $\phi_h(z)$ in (5), and $E_{\rm th} = 6$ keV.

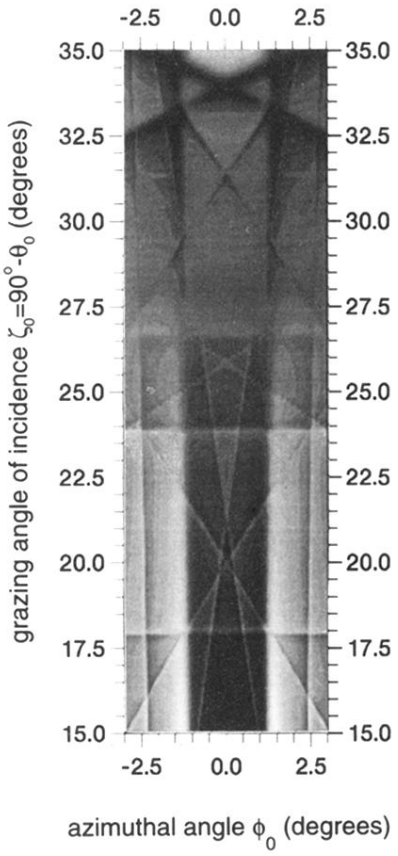

FIG. 7. Intensity distribution in the channeling pattern computed numerically for the (001) face of a single crystal of Si and for a high-angle position of the detector (Ref. 15), namely, $\zeta = 50^\circ$ and $\phi = 180^\circ$. The azimuth $\phi_0 = 0$ is parallel to the (220) planes, and $E_0 = 25$ keV. Calculations have been performed using 14 terms of the expansion (16) and 26 functions $\phi_h(z)$ in (5), and $E_{\rm th} = 6$ keV. Note the effect of reversal of the contrast of the band at $\zeta_c \approx 26^\circ$.